© 2015. Published by The Company of Biologists Ltd | Journal of Cell Science (2015) 128, 1279–1293 doi:10.1242/jcs.154443

RESEARCH ARTICLE

Self-organization of core Golgi material is independent of COPII-mediated endoplasmic reticulum export

Christian E. Schuberth[1,2,3,§], Carolina Tängemo[1,*], Cvetalina Coneva[1,‡], Christian Tischer[4] and Rainer Pepperkok[1,4]

ABSTRACT

The Golgi is a highly organized and dynamic organelle that receives and distributes material from and to the endoplasmic reticulum (ER) and the endocytic pathway. One open question about Golgi organization is whether it is solely based on ER-to-Golgi transport. Here, we analyzed the kinetics of Golgi breakdown in the absence of COPII-dependent ER export with high temporal and spatial resolution using quantitative fluorescence microscopy. We found that Golgi breakdown occurred in two phases. While Golgi enzymes continuously redistributed to the ER, we consistently observed extensive Golgi fragmentation at the beginning of the breakdown, followed by microtubule-dependent formation of a Golgi remnant structure (phase 1). Further Golgi disintegration occurred less uniformly (phase 2). Remarkably, cisternal Golgi morphology was lost early in phase 1 and Golgi fragments instead corresponded to variably sized vesicle clusters. These breakdown intermediates were devoid of COPI-dependent recycling material, but contained typical 'core' Golgi components. Furthermore, Golgi breakdown intermediates were able to disassemble and reassemble following cell division, indicating that they retained important regulatory capabilities. Taken together, these findings support the view that Golgi self-organization exists independently of ER-to-Golgi transport.

KEY WORDS: Sar1, Golgi dynamics, Live-cell imaging, Secretory pathway

INTRODUCTION

The Golgi in mammalian cells is a highly organized organelle that consists of several stacks of flattened, membrane-bounded cisternae that interconnect to form the Golgi ribbon (Klumperman, 2011; Lowe, 2011; Nakamura et al., 2012). Despite its static appearance, the Golgi is a very dynamic organelle. During cell division, the Golgi ribbon and, subsequently, the cisternal structure of the stacks break apart and separate into small entities that are inherited by the daughter cells to reform a new Golgi complex (Shorter and Warren, 2002; Wei and Seemann, 2009). Furthermore, during normal secretory transport in interphase cells, the Golgi receives, sorts and exchanges proteins and lipids with the endoplasmic reticulum (ER) and the endosomal system (Derby and Gleeson, 2007; Pavelka et al., 2008). In this respect, continuous transport from the ER to the Golgi has been described as essential for the maintenance of the Golgi complex. For example, inhibition of COPII function with dominant-negative mutants of the small GTPase Sar1 (Sar1^{dn}, which can be Sar1^{GTP} or Sar1^{GDP}) leads to a block of ER export and the redistribution of Golgi enzymes to the ER (Shima et al., 1998; Storrie et al., 1998; Zaal et al., 1999). This supports a model of Golgi organization in interphase cells that is based on continuous cycling of Golgi material through the ER. However, the idea has been questioned by a study showing that Golgi enzymes do not cycle through the ER in cells under normal conditions (Pecot and Malhotra, 2006). In addition, certain structural Golgi proteins like GM130 or GRASP65 (also known as GOLGA2 and GORASP1, respectively) were found in discrete structures that are distinct from the ER after Sar1^{GTP} treatment, showing that not all Golgi material merges with the ER. These components were proposed to constitute a Golgi matrix that provides a level of Golgi self-organization independent of ER-to-Golgi transport (Kasap et al., 2004; Puri et al., 2004; Seemann et al., 2000; Seemann et al., 2002). However, formation of the Golgi matrix was only observed when ER transport was blocked with Sar1^{GTP} mutants, but not with Sar1^{GDP} mutants (Kasap et al., 2004; Miles et al., 2001; Seemann et al., 2000; Stroud et al., 2003; Ward et al., 2001), raising concerns about the Golgi matrix model. In summary, a number of studies have been performed to date looking at different Golgi markers at different time-points after blocking ER export by inhibiting the small GTPase Sar1. However, interpretation of the results of 'snapshots' of Golgi breakdown processes have led to contradictory conclusions about the self-organization ability of the Golgi complex in mammalian cells (Girod et al., 1999; Miles et al., 2001; Prescott et al., 2001; Seemann et al., 2000; Seemann et al., 2002; Shima et al., 1998; Storrie et al., 1998; Stroud et al., 2003; Ward et al., 2001; Zaal et al., 1999). Here, we analyzed the impact of both Sar1 mutants on the kinetics of Golgi breakdown in mammalian cells by quantitative live-cell imaging, to gain better insight into how much Golgi organization is based on ER-to-Golgi transport.

RESULTS

To efficiently induce a robust ER export block, we used an adenovirus system to express dominant-negative Sar1 mutants in HeLa cells (Yoshimura et al., 2004) – Sar1H79G and Sar1T39N, referred to as Sar1^{GTP} and Sar1^{GDP}, respectively. Owing to the

[1]Cell Biology and Biophysics Unit, European Molecular Biology Laboratory (EMBL), Meyerhofstr. 1, 69117 Heidelberg, Germany. [2]Institute of Cell Dynamics and Imaging, University of Muenster, von-Esmarch-Str. 56, 48149 Muenster, Germany. [3]Cells in Motion Cluster of Excellence (EXC1003-CiM), University of Muenster, von-Esmarch-Str. 56, 48149 Muenster, Germany. [4]Advanced Light Microscopy Facility, European Molecular Biology Laboratory (EMBL), Meyerhofstr. 1, 69117 Heidelberg, Germany.
*Present address: Centre for Cellular Imaging, University of Gothenburg, Medicinaregatan 7A, 40530 Gothenburg, Sweden. ‡Present address: Max Planck Institute of Neurobiology, Am Klopferspitz 18, 82152 Martinsried, Germany.

§Author for correspondence (cschuber@uni-muenster.de)

Received 3 April 2014; Accepted 28 January 2015

Journal of Cell Science

fact that Sar1 mutants are toxic for virus packaging cells, the expression system has been developed such that a virus coding for a silenced Sar1 mutant can be activated for expression by co-infection with a second virus coding for the Cre recombinase (Yoshimura et al., 2004). Thus, $Sar1^{GTP}$ and $Sar1^{GDP}$ virus infections in our experiments will correspond to $Sar1^{GTP}$+Cre and $Sar1^{GDP}$+Cre double virus infections, respectively, unless otherwise stated. Optimization of experimental conditions allowed us to obtain 98.2%±0.3% and 83.9%±3.5% (±s.e.m.) of HeLa cells showing a complete Golgi redistribution phenotype at 20 h post-infection for $Sar1^{GTP}$ and $Sar1^{GDP}$ virus-infected cells, respectively. Similar results were reported in the previous study (Yoshimura et al., 2004). However, ∼4 h after $Sar1^{GTP}$ virus infection we could already detect significant amounts of $Sar1^{GTP}$ in HeLa cell extracts by western blotting and in single cells by immunofluorescence analysis (supplementary material Fig. S1A,B). To test the efficiency of the Sar1 mutants, we performed secretory transport assays with the model cargo VSVG–YFP (Presley et al., 1997). We found ER export of VSVG–YFP to be completely blocked in 87% (n=212) of HeLa cells as early as 3:35 h after $Sar1^{GTP}$ virus infection (supplementary material Fig. S1C,D). The $Sar1^{GDP}$ infection took slightly longer to generate the transport block, rising from 15% (n=248) of cells at 3:30 h post-infection to 65% (n=37) at 6:00 h post-infection, indicating that the $Sar1^{GDP}$ mutant needs higher expression levels to achieve the full transport block. Importantly, within the fraction of $Sar1^{GDP}$-expressing cells with VSVG–YFP accumulation in the ER, we did not observe any intracellular transport structures (i.e. VSVG–YFP signal concentrated on top of the diffuse ER staining) or plasma membrane staining when we analyzed these cells by fluorescence microscopy (supplementary material Fig. S1E). Thus, once induced, the ER export block was complete and remained stable over time. In addition, we could not detect any post-ER structures after $Sar1^{GTP}$ virus infection for other cargoes like GPI–YFP or the YFP-labeled EGF receptor (not shown).

Golgi breakdown after ER export block occurs in two phases

We then infected HeLa cells stably expressing the Golgi marker GalNAc-T2–GFP (Storrie et al., 1998) with $Sar1^{GTP}$ virus and followed the changes in Golgi morphology by time-lapse fluorescence microscopy (Fig. 1A; supplementary material Movie 1). At ∼3 h after infection, the Golgi started to fragment into numerous heterogeneously sized structures that were initially observed in close proximity to the Golgi and then became distributed throughout the cell (Fig. 1A). To elucidate the origin of the small GalNAc-T2–GFP-positive structures, we performed spinning-disk live-cell microscopy at one image per second. With this temporal resolution we were able to frequently observe smaller GFP structures or tubules emerging from larger fragments (Fig. 1B), indicating that most GFP-labeled fragments were Golgi-derived. After the initial fragmentation, most of the smaller structures disappeared over time, along with a steady increase in the GFP signal in the ER (Fig. 1A). This suggests that these structures were redistributing to the ER. Surprisingly, GalNAc-T2–GFP structures remaining after the initial fragmentation re-clustered in the perinuclear area and formed a larger Golgi-like structure that we termed a ‘Golgi remnant’ (Fig. 1A). The Golgi remnant broke apart again into smaller fragments and disintegrated, until eventually all the GFP signal was redistributed to the ER (Fig. 1A). This sequence of events was evident for all $Sar1^{GTP}$-expressing cells analyzed and was also observed in $Sar1^{GDP}$-expressing cells (supplementary material Fig. S2A; supplementary material Movie 2). Importantly, single infection of cells with only Cre or silent Sar1 mutant viruses had no effect on Golgi morphology within the 20-h observation period (Fig. 3A; Fig. 4A; data not shown).

To analyze and compare the obtained movies of Golgi breakdown, we developed an image segmentation algorithm termed ‘MorphoQuant’ (supplementary material Fig. S1G; MatLab code at https://github.com/tischi/MorphoQuant). This allowed robust identification of Golgi fragments within cells, even on top of an increasing background signal (i.e. ER). We extracted several parameters from the program to quantify the behavior of GFP-labeled Golgi material during Golgi breakdown (Fig. 1C–F). Interestingly, we found pronounced changes in the number of Golgi fragments over time, along with a corresponding change in their mean size (Fig. 1C). By contrast, the Golgi signal decay and the signal increase outside of Golgi fragments (reflecting mainly the ER signal) were rather continuous (Fig. 1D). This demonstrated that the dynamic changes in Golgi fragment number were uncoupled from the steady loss of Golgi material. Furthermore, the mean fluorescence signal of Golgi fragments and the maximum signal within the largest fragment indicated that different modes of Golgi redistribution exist in the course of the breakdown (Fig. 1E). These findings suggest that Golgi breakdown can be subdivided into different phases, which we decided to define by using the number of Golgi fragments as a parameter (Fig. 1C; Table 1). A sharp increase in Golgi fragment number consistently marked the start of Golgi breakdown, which also coincided with the start of Golgi signal decay (Fig. 1C,D). After time periods of 3.1±0.6 h for $Sar1^{GTP}$ and 4.8±0.8 h for $Sar1^{GDP}$, the number of fragments dropped to a local minimum and marked the end of the first breakdown phase (Phase 1; Fig. 1C–F). At this time-point, 9 out of 12 $Sar1^{GTP}$- and 4 out of 8 $Sar1^{GDP}$-expressing cells formed pronounced Golgi remnants, so we decided to call this the remnant time-point (RTp; Fig. 1C–F). The remaining time interval up to the end of the breakdown process (i.e. number of Golgi fragments continuously ≤3) was defined as the second phase (Phase 2; Fig. 1C–F). For all cells imaged we were able to identify two Golgi breakdown phases, and the obtained breakdown parameters are summarized in Table 1.

Next, we wanted to score in a quantitative way for the ability of Golgi fragments to reform a Golgi remnant during Golgi breakdown. To this end, we analyzed the area of the largest Golgi fragment identified at each time-point. This value dropped at the onset of the process, but increased again 6 h post-infection and displayed a local maximum at 7–8 h post-infection (Fig. 1F). Notably, in the same time frame, the total area occupied by Golgi fragments decreased (Fig. 1F). To evaluate Golgi fragment re-association, we compared the maximum value of the largest Golgi fragment found in phase 2 (Fig. 1F, value C) with the smallest value in phase 1 (Fig. 1F, value B), generating a Golgi re-clustering index C/B. Like this, an index larger than 1 would immediately indicate that a larger Golgi structure was formed from smaller structures. Remarkably, we found re-clustering indices ranging from 1.2 to 8.8 for all cells analyzed, independent of the type of Sar1 mutant expressed (Fig. 1G; Table 1). We also determined the efficiency of re-clustering, i.e. we compared the size of the reformed Golgi remnant (Fig. 1F, value C) to the average size of large Golgi structures before breakdown (Fig. 1F, value A). Interestingly, we found that the reformed Golgi structure could reach the same approximate size in

Journal of Cell Science (2015) 128, 1279–1293 doi:10.1242/jcs.154443

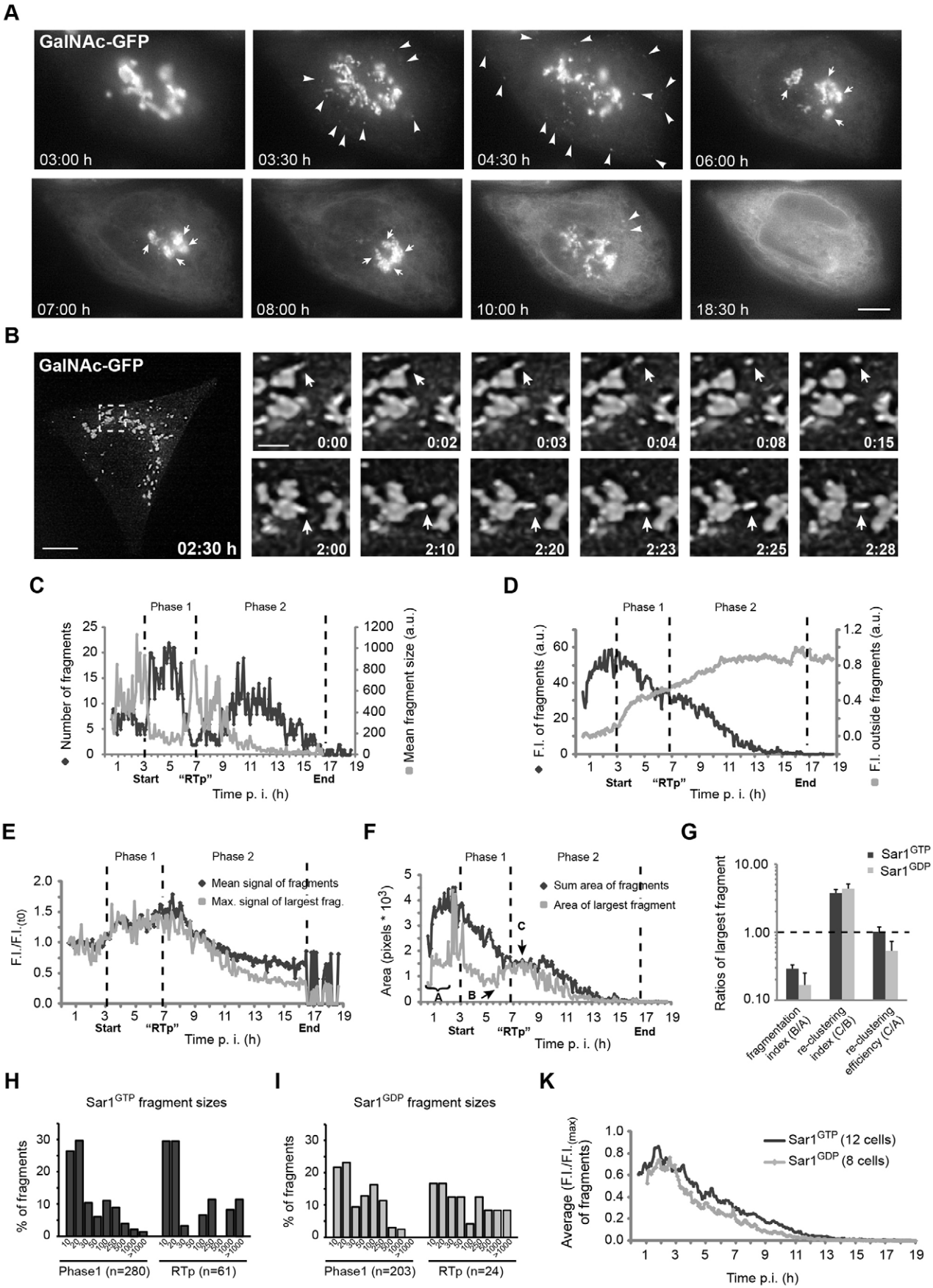

Fig. 1. See next page for legend.

Journal of Cell Science

Journal of Cell Science (2015) 128, 1279–1293 doi:10.1242/jcs.154443

Fig. 1. Golgi breakdown and GalNac-T2–GFP redistribution to the ER after Sar1 mutant expression. (A,B) HeLa cells stably expressing GalNAc-T2–GFP were infected with $Sar1^{GTP}$ adenovirus and followed by time-lapse fluorescence microscopy on a widefield system every 5 min (A) or on a spinning-disk confocal microscope every second (B). (A) Arrowheads point to GalNAc-T2–GFP structures in the periphery of the cell. Arrows indicate larger GalNAc-T2–GFP structures that re-cluster in the perinuclear area. The gamma value for the GFP signal was enhanced similarly for all pictures to highlight the accumulation of GalNAc-T2–GFP in the ER. Scale bar: 5 μm. (B) Arrows point to smaller GalNAc-T2–GFP structures separating from larger fragments. Scale bars: 10 μm (main image), 2 μm (zoom). (C–F) GFP signal parameters obtained by MorphoQuant analysis of images in A plotted over time post-infection (p.i.). (C) The number of GalNAc-T2–GFP fragments (black curve) and the mean size of fragments (gray curve). a.u., arbitrary units. (D) Total fluorescence intensity (F.I.) within GFP fragments (black curve) and fluorescence intensity increase outside of the fragments (gray curve). (E) Mean fluorescence signal of GFP fragments (black curve) and maximum signal of largest fragment (gray curve). (F) The sum of the area of all GFP fragments (black curve) and the area of the largest fragment for each time-point (gray curve). (F,G) Three values of the area of the largest GalNAc-T2–GFP fragment were determined for all cells: the mean value ≤2 h post infection ('A'), the smallest value in phase 1 ('B') and the largest value in phase 2 ('C'). (G) Ratios for Golgi fragmentation (B/A), Golgi re-clustering (C/B) and Golgi re-clustering efficiency (C/A) are plotted. Data show the mean±s.e.m. for 12 cells after $Sar1^{GTP}$ and 8 cells after $Sar1^{GDP}$ virus infection. (H,I) Histograms of fragment size distributions in phase 1 and at the remnant time-point for cells expressing $Sar1^{GTP}$ (H) and $Sar1^{GTP}$ (I). (K) Mean Golgi signal decay of 12 cells expressing $Sar1^{GTP}$ (black curve) and 8 expressing $Sar1^{GDP}$ (gray curve).

$Sar1^{GTP}$-expressing cells and around half the size in $Sar1^{GDP}$-expressing cells (Fig. 1G; Table 1). Furthermore, re-clustering of Golgi fragments was evident when we compared fragment size distributions from cells in phase 1 and at the RTp (Fig. 1H,I). Thus, Golgi fragment re-clustering is a substantial phenomenon during Sar1-mutant-induced Golgi breakdown. To complement our analysis, we scored for Golgi fragmentation (Fig. 1F,G; Table 1). The obtained values between 0.1 and 0.7 corresponded well to the Golgi dispersal observed in phase 1. Taken together, we found that Golgi breakdown in $Sar1^{GTP}$- and $Sar1^{GDP}$-expressing cells occurred in similar ways, i.e. through two breakdown phases with strong re-clustering activities of the intermediately produced Golgi fragments. Differences between Sar1 mutants can be found in redistribution kinetics and Golgi fragment dynamics (Fig. 1G–K; Table 1).

To control for the Golgi marker and the Sar1 expression system used, we infected GalT–GFP-expressing cells with $Sar1^{GTP}$ virus and analyzed GalNAc-T2–GFP-expressing cells after mCherry–$Sar1^{GTP}$ plasmid transfection. In both experiments, we observed a biphasic Golgi breakdown pattern with Golgi fragment re-clustering, similar to the previous experiments. Re-clustering indices were 4.0±0.6 (n=9) for $Sar1^{GTP}$-virus-infected GalT–GFP cells and 3.3±1.0 (n=6) for $Sar1^{GTP}$-plasmid-transfected GalNAc-T2–GFP cells.

Golgi fragment re-clustering is microtubule dependent

It is well established that the microtubule network in mammalian cells is necessary for the perinuclear localization of the Golgi complex (Sandoval et al., 1984; Thyberg and Moskalewski, 1985; Wehland et al., 1983). Therefore, we investigated the role of microtubules in the re-clustering of Golgi fragments. Sar1-mutant-induced Golgi redistribution to the ER has been shown to occur in cells treated with the microtubule-depolymerizing drug nocodazole (Shima et al., 1998; Storrie et al., 1998). Golgi breakdown was also observed in our experiments when 10 μM nocodazole was added either directly or 2:40 h after $Sar1^{GTP}$ virus infection, or 1:10 h after $Sar1^{GDP}$ infection (Fig. 2A–D). However, no long-range movement of Golgi fragments was observed, only some re-clustering on the scale of a few micrometers (Fig. 2A). When we analyzed the area of the largest Golgi fragment over time, we found that the previously defined re-clustering index for Golgi fragments gave large values (>3) only for non-treated cells, whereas in the presence of nocodazole it remained at 1.1±0.1 for $Sar1^{GTP}$ and 1.9±0.3 for $Sar1^{GDP}$ (Fig. 2C,D). Importantly, when we removed the drug after cells had entered phase 1, we could restore Golgi fragment re-clustering in the perinuclear area (Fig. 2E). Thus, an intact microtubule network is important for Golgi fragment re-clustering during Sar1-mutant-induced Golgi breakdown.

Golgi fragments are clusters of vesicle-like structures

Next, we wanted to investigate the GFP-labeled Golgi fragments on the ultrastructural level by correlative fluorescence and electron microscopy (Colombelli et al., 2008; Tängemo et al., 2011). GalNAc-T2–GFP-expressing cells were followed by fluorescence microscopy after $Sar1^{GTP}$ virus infection, fixed at different breakdown phases and processed and analyzed by electron microscopy (Fig. 3A). Remarkably, already at early time-points of Golgi fragmentation in phase 1 (4 h post-infection), we found that the cisternal morphology of the Golgi was lost. The fragments observed by fluorescence microscopy corresponded to clusters of vesicle-like structures (Fig. 3A). Analyzing whole cells by serial sectioning revealed several of these clusters per section at 4 h post-infection. They were composed of ~50–150 vesicular structures of similar sizes, mostly with diameters <80 nm (Fig. 3A,B). The Golgi remnant observed by fluorescence microscopy at 7 h post-infection also corresponded to an accumulation of vesicle-like structures. However, all structures were tightly connected to each other and formed one continuous cluster (Fig. 3A). Within this cluster, we could detect vesicular structures with significantly larger diameters (>200 nm) compared to the structures observed at the earlier time-point (Fig. 3A,B), suggesting that smaller vesicular structures are fusing when the Golgi remnant is formed. For the $Sar1^{GDP}$ mutant, the correlative fluorescence and electron microscopy analysis revealed very similar morphological phenotypes (Fig. 3C; supplementary material Fig. S2B).

Golgi breakdown intermediates are depleted of COPI-dependent components

The rapid loss of the cisternal morphology made us wonder about the identity of GalNAc-T2–GFP-labeled Golgi breakdown intermediates. To address this, we performed immunofluorescence experiments using a variety of markers for the Golgi complex and Golgi-to-ER transport. Importantly, no overlap of GalNAc-T2–GFP fragments with endosomal, lysosomal or ER markers could be detected (data not shown), indicating that the GFP-labeled fragments represent only Golgi or Golgi-derived material. First, we analyzed the effect of the Sar1-mutant-induced ER export block on the localization of proteins known to continuously recycle between the Golgi and the ER – the KDEL receptor (KDELR1–3) and the p24 protein family member p24γ3 (p27, also known as TMED7) (Blum et al., 1999; Füllekrug et al., 1999). Both markers lost their juxtanuclear localization early after Sar1 mutant expression, as shown for $Sar1^{GDP}$-expressing cells in Golgi breakdown phase 1 (Fig. 4A,B). Next, we analyzed the breakdown intermediates for

Journal of Cell Science (2015) 128, 1279–1293 doi:10.1242/jcs.154443

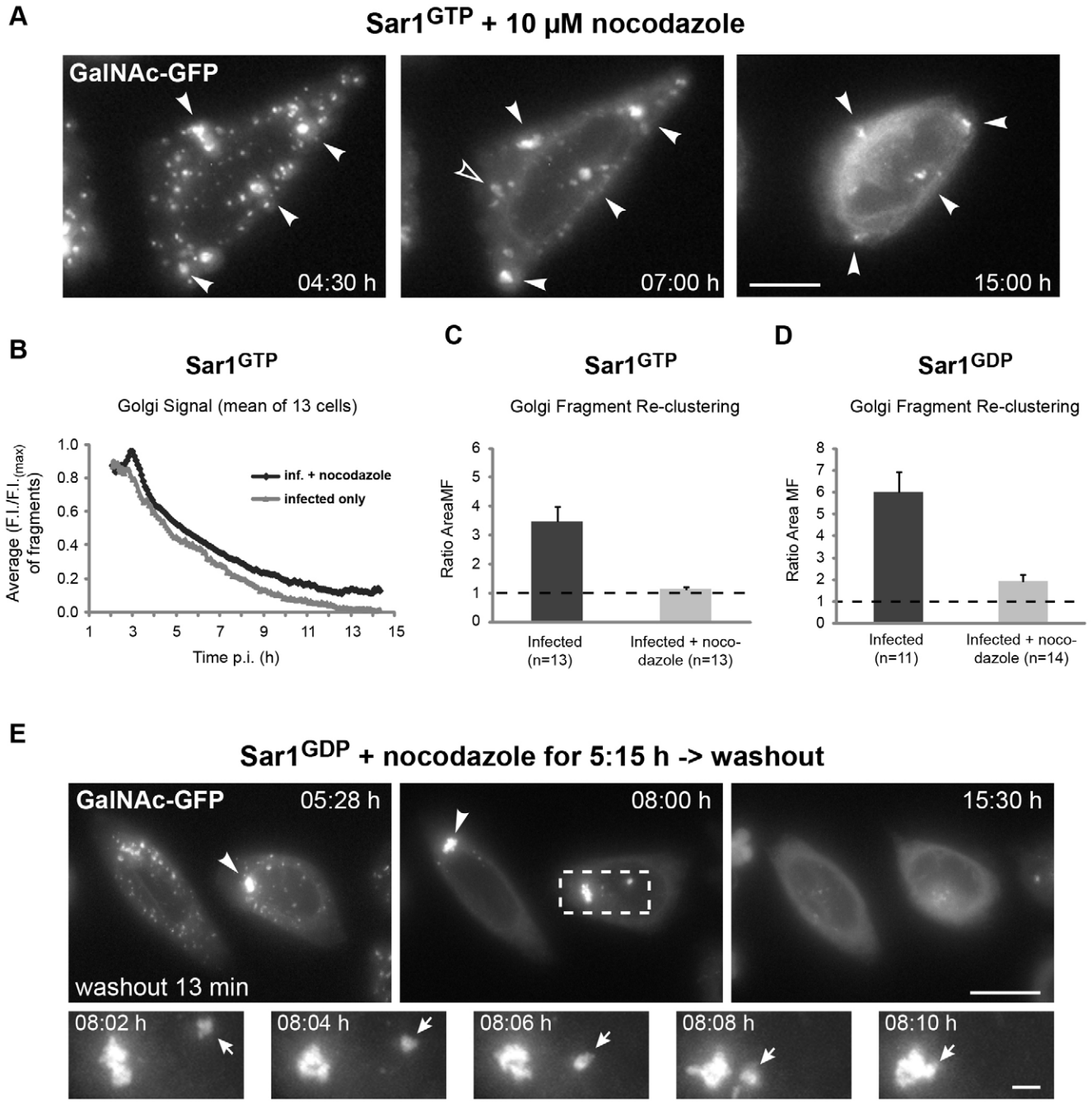

Fig. 2. Golgi fragment re-clustering depends on an intact microtubule network. (A–C) HeLa cells stably expressing GalNAc-T2–GFP were infected with $Sar1^{GTP}$ adenovirus and followed by time-lapse fluorescence microscopy. (A) Image gallery of GalNAc-T2–GFP redistribution in the presence of 10 µM nocodazole. Closed arrowheads indicate immobile Golgi structures; the open arrowhead indicates locally restricted re-clustering. (B) Mean GalNAc-T2–GFP signal decay of Golgi fragments measured by MorphoQuant in the presence and absence of 10 µM nocodazole. F.I., fluorescence intensity; p.i. post-infection. (C) Golgi fragment re-clustering indices of cells analyzed in B. MF, maximum-size fragment. (D) Golgi fragment re-clustering indices for cells infected with $Sar1^{GDP}$ virus in the absence or presence of 10 µM nocodazole. Data show the mean±s.e.m. (E) Dynamics of GalNAc-T2–GFP fragments in $Sar1^{GDP}$ cells after nocodazole washout. Arrowheads indicate reformed Golgi remnants; the arrow in the zoomed image sequence marks trafficking of a GalNAc-T2–GFP fragment. Scale bars: 10 µm (A,E, main image), 2 µm (zoom).

the presence of the COPI coat machinery, which is involved in the transport of KDEL receptor and p24. We found a partial overlap of β′-COP labeling on large (66%) and small GFP fragments (44%) in phase 1 and β′-COP signal on around half of the reformed Golgi remnants (Fig. 4C; Fig. 5B–D). As COPI is one of the major targets of the drug brefeldin A (BFA) (Donaldson et al., 1990; Scheel et al., 1997), the loss of COPI cargo and partial loss of COPI coat raised the question of whether the Golgi breakdown intermediates would still be sensitive to BFA. Under normal conditions, BFA treatment leads to a fast redistribution of Golgi enzymes to the ER in mammalian cells (Donaldson et al., 1990; Lippincott-Schwartz et al., 1989; Orci

Journal of Cell Science (2015) 128, 1279–1293 doi:10.1242/jcs.154443

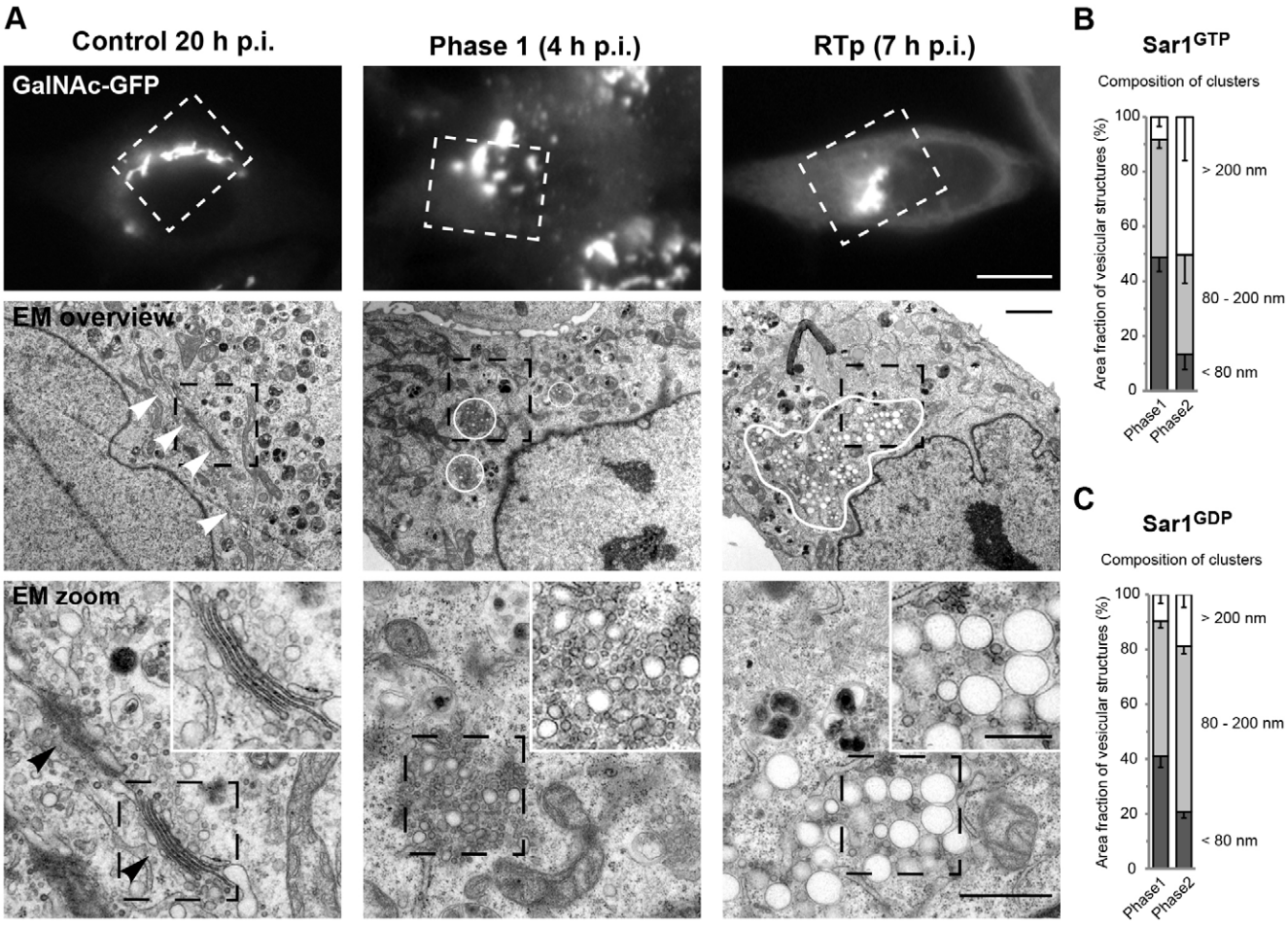

Fig. 3. Golgi fragments observed after Sar1 mutant expression are clusters of vesicle-like structures. (A) HeLa cells stably expressing GalNAc-T2–GFP were infected with Sar1^{GTP} virus only (control) or Sar1^{GTP} and Cre viruses and imaged by fluorescence microscopy. Cells showing typical GalNAc-T2–GFP morphology for phase 1 [4 h post-infection (p.i.)] or with remnants (7 h post-infection) were fixed and subjected to electron microscopy (EM) analysis. At the region corresponding to the obtained fluorescence signal (white dashed rectangles), Golgi stacks (white arrowheads) or vesicular clusters (white circles, white shape) corresponding to the fluorescence signal could be identified and are shown at higher magnification (black dashed rectangles, middle panel). Black arrowheads indicate individual Golgi stacks. Scale bars: 10 µm (upper panels), 2 µm (middle panels), 1 µm (lower panels), 500 nm (lower panels, insets). (B) The composition of vesicular clusters at 4 h (Phase 1, nine clusters of three cells) and 7 h (Phase 2, remnants of three cells) post Sar1^{GTP} and Cre infection. (C) Composition of vesicular clusters in cells after 5 h (Phase 1, five clusters of two cells) and 8 h (Phase 2, remnants of three cells) post Sar1^{GDP}and Cre infection. Data are given as the mean±s.e.m.

et al., 1991). In Sar1^{GTP}- and Sar1^{GDP}-expressing cells, by contrast, Golgi fragments in phase 1 were partially resistant and Golgi remnants completely resistant to BFA treatment (Fig. 4D,E). This suggests that not only fast recycling cargo, but proteins and lipids important for BFA-mediated tubule formation and retrograde Golgi-to-ER trafficking are depleted from Golgi breakdown intermediates.

Molecular composition of Golgi breakdown intermediates

In the course of the colocalization analysis, we observed significant differences between Sar1^{GTP}- and Sar1^{GDP}-expressing cells in the co-labeling of GalNAc-T2–GFP structures. Sar1^{GDP} expression led to a loss of the COPII component Sec13 from Golgi membranes (Fig. 5A) and this loss was more pronounced on Golgi remnants (Fig. 5A,B). By contrast, Sar1^{GTP}-expressing cells showed a strong labeling of Sec13 close to and on top of the Golgi fragments in phase 1, and on the Golgi remnant (Fig. 5A,C). The close association of COPII with Golgi membranes appeared to have an impact on ERGIC53, COPI and p24 localization in phase 2 and, to a lesser extent, on late Golgi markers like TGN46 (also known as TGOLN2) (Fig. 5B,C). At the final time-point, when all GalNAc-T2–GFP has been redistributed to the ER, the different behavior of COPII resulted in a Sar1^{GTP}-dependent clustering of a number of Golgi and transport markers (supplementary material Fig. S3). The latter finding has been reported before and led to controversial discussions on the putative functions of these clusters (Seemann et al., 2000; Seemann et al., 2002; Stroud et al., 2003; Ward et al., 2001; Yoshimura et al., 2004; Zaal et al., 1999). Therefore, we decided to focus our colocalization analysis on Sar1^{GDP}-induced Golgi breakdown intermediates (Fig. 5A,B,D,E), as their composition is not affected by an accumulation of COPII coat. In phase 1 cells, we found that all large and more than half of the small GalNAc-T2–GFP structures were positive for Golgi components of various types: Golgi enzymes [GalNAc-T2 (also known as GALNT2), GalT], golgins with different functions [structural and stacking proteins, proteins for vesicle tethering;

Journal of Cell Science (2015) 128, 1279–1293 doi:10.1242/jcs.154443

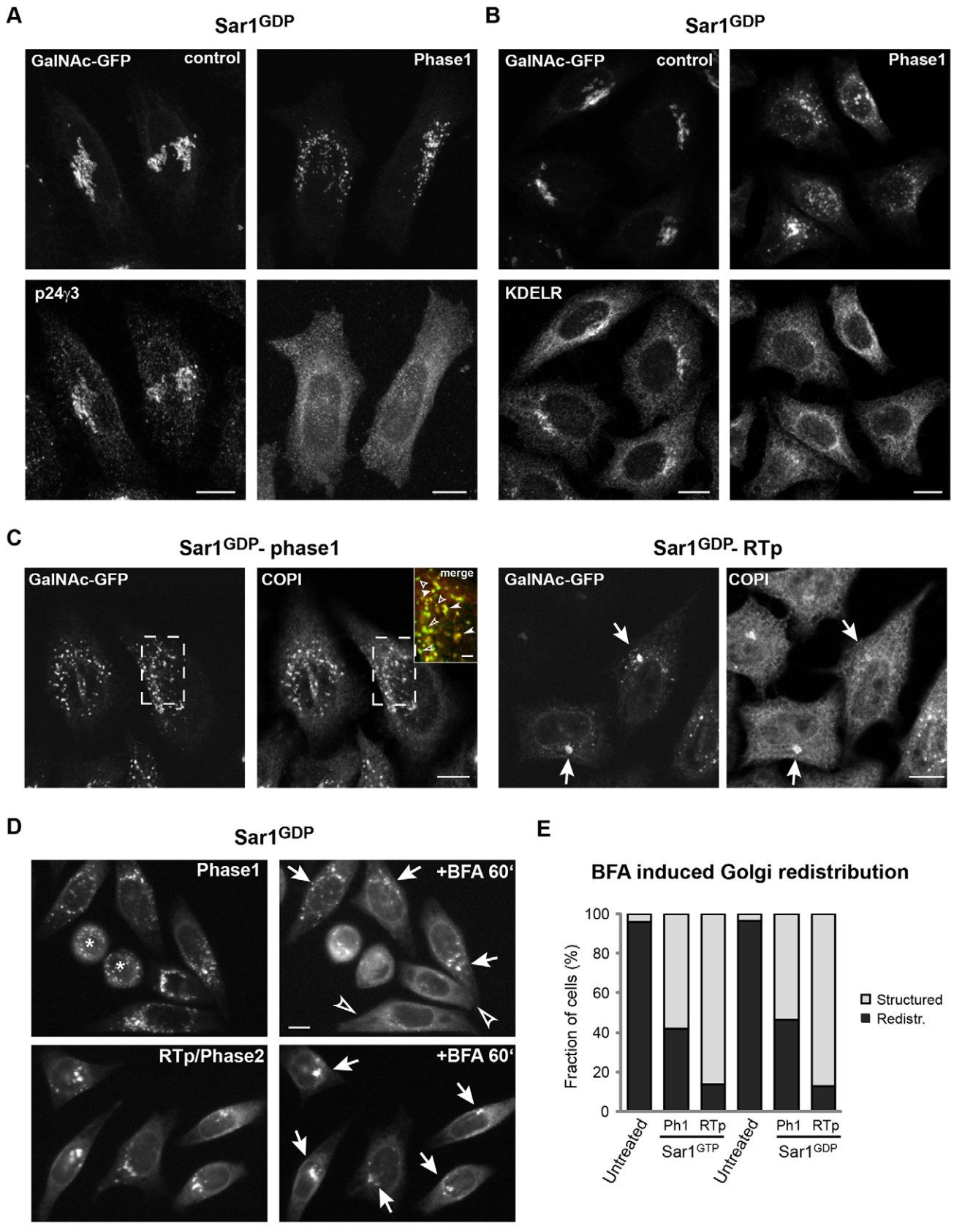

Fig. 4. See next page for legend.

Fig. 4. GalNAc-T2–GFP fragments lose COPI and recycling cargo and are resistant to treatment with brefeldin A. (A–C) HeLa cells stably expressing GalNAc-T2–GFP were infected with $Sar1^{GDP}$ only (control) or $Sar1^{GDP}$ and Cre adenoviruses, fixed at 5 h post-infection and stained for p24γ3 (A) or the KDEL receptor (B), or fixed at 5 h and 8 h post-infection and stained for COPI (C). Closed arrowheads point to GalNAc-T2–GFP structures with overlapping COPI signal; open arrowheads indicate structures with GFP signal only. Long and short arrowheads distinguish between large and small GalNAc-T2–GFP structures. Arrows indicate reformed Golgi remnants. (D) HeLa cells stably expressing GalNAc-T2–GFP were infected with $Sar1^{GDP}$ and Cre adenoviruses and followed by time-lapse fluorescence microscopy. At the indicated phases of breakdown, 5 mg/ml brefeldin A was added to the medium and the cells were continuously imaged for 1 h to check for combined effects of the drug and $Sar1^{GDP}$ expression. Open arrowheads indicate cells with redistributed GalNAc-T2–GFP signal; arrows indicate cells with Golgi fragments or Golgi remnants; asterisks mark two daughter cells of a previous cell division.
(E) Quantification of data shown in D and an experiment with $Sar1^{GTP}$. Cells with structured or redistributed Golgi appearance were counted ($Sar1^{GTP}$, $n=329$, $n=50$ and $n=43$ for untreated, phase 1 and RTp/phase 2, respectively; $Sar1^{GDP}$, $n=60$, $n=41$ and $n=135$). Scale bars: 10 μm (A–D), 2 μm (C, inset).

GM130, GRASP65, giantin (also known as GOLGB1) and p115], Golgi-localized SNAREs [GS28 (also known as GOSR1), syntaxin5] and a Golgi GTPase (Rab6) (Fig. 5B–D). These markers were also present on the reformed Golgi remnants (structures >1 μm at RTp and phase2, Fig. 5B). In addition, ERGIC53, golgin97 (also known as GOLGA1) and TGN46 were also detected on the remnant (>70%, Fig. 5B). Given that these markers were present on only 30–50% of large and small GalNAc-T2–GFP structures in phase 1 (Fig. 5B,D), one can speculate that it is predominantly these fragments that reform the Golgi remnant.

We always found a subset of small GalNAc-T2–GFP-positive structures showing no colocalization with the Golgi markers tested (Fig. 5A,D). To characterize their identity, we performed double immunofluorescence labeling with different combinations of markers for Golgi structural components (GM130, GRASP65), Golgi enzymes (GalT) and proteins related to transport (COPI, SNAREs GS28 and syntaxin5) (Fig. 5E). Analysis of co-labeling for each marker individually and both markers simultaneously revealed different patterns of signal overlap on the GalNAc-T2–GFP structures for different marker combinations (Fig. 5E). For example, more GalNAc-T2–GFP structures were labeled in total in the GalT and GRASP65 experiment than in the GM130 and GRASP65 experiment (Fig. 5E). This suggests that during Golgi breakdown, a population of Golgi-enzyme-containing fragments is generated that is distinct from GM130, GRASP65 and GalNAc-T2–GFP fragments. By contrast, we found fewer double-labeled GalNAc-T2–GFP structures for GM130 and COPI than for other marker combinations (Fig. 5E), indicating that a distinction can be drawn between pure Golgi and Golgi-transport-related small fragments. Importantly, the co-labeling results suggest that GalNAc-T2–GFP structures are not randomly generated Golgi fragments, but reflect certain subclasses of Golgi-derived material. Taken together, we find that most Golgi breakdown intermediates and, in particular, the Golgi remnant contained all the typical Golgi markers tested, underlining their Golgi origin and identity.

Golgi breakdown intermediates are able to disassemble and reassemble during cell division

In mammalian cells, Golgi inheritance involves a complete breakdown and reassembly of the Golgi ribbon and the stacked cisternal structure (Wei and Seemann, 2009; Wei and Seemann, 2010). During this process, Golgi fragments of various sizes are generated, and vesicular clusters have been described as units of Golgi inheritance (Jokitalo et al., 2001; Lucocq et al., 1987; Misteli and Warren, 1995; Shima et al., 1997). Therefore, we first wanted to test the co-labeling of Golgi markers on mitotic Golgi structures as we did for Golgi breakdown intermediates (Fig. 6). Interestingly, we found that during cell division more small GalNAc-T2–GFP fragments were positive for GalT than for GRASP65 (Fig. 6A,B). Furthermore, significantly different patterns of GalT/GRASP65, GM130/GRASP65 and GM130/COPI marker overlap on small GalNAc-T2–GFP fragments were

Table 1. Golgi breakdown kinetics and Golgi fragment dynamics

	$Sar1^{GTP}$	$Sar1^{GDP}$
Start (hh:mm)[a]	2:26±0:20	3:07±0:25
Remnant time-point (hh:mm)[a]	5:33±0:40	7:54±0:47
End (hh:mm)[a]	14:15±2:29	12:43±2:33
Duration Phase 1 (h)	3.1±0.6	4.8±0.8
Duration Phase 2 (h)	8.7±2.2	4.8±2.7
Estimated half time (h)[b]	1.8±0.5	1.4±0.6
Number of structures (mean <2 h)	8.6±1.4	4.0±0.7
Max. structures (Phase 1)	23.6±2.4	25.3±2.0
Increase (fold)	3.2±0.4	7.3±0.9
Increase time (min)[c]	31.3±4.0	48.8±6.2
Decrease to initial number (min)[d]	100.0±10.5	200.0±20.0
Fragmentation index[e]	0.29±0.04	0.17±0.08
Re-clustering index[f]	3.75±0.47	4.35±0.73
Re-clustering efficiency[f]	1.02±0.17	0.53±0.20

[a]The parameter of the number of fragments were used to determine the starting point (steady increase in number towards the maximum), the remnant time point [local minimum with the same value (±1) as before the start] and the end time-point (no large structures and small structures ≤3). [b]The time from the start of Golgi signal decay to the first time-point where signal is ≤50% of the start value and continuously descending for at least 5 time-points. [c]The time interval between the starting point and the (first) time-point of maximum number of fragments. [d]The time interval between the (last) time-point of maximum number and the remnant time-point. [e]The ratio of the minimum value of the area of the largest GFP fragment identified in phase 1 over the mean of this value ≤2 h. [f]The ratio of the maximum value of the area of the largest GFP fragment identified in phase 2 over the minimum value in phase 1 (re-clustering index) or the mean value ≤2 h (reclustering efficiency). [a–d]Values are mean±s.d., others are mean±s.e.m.

Journal of Cell Science (2015) 128, 1279–1293 doi:10.1242/jcs.154443

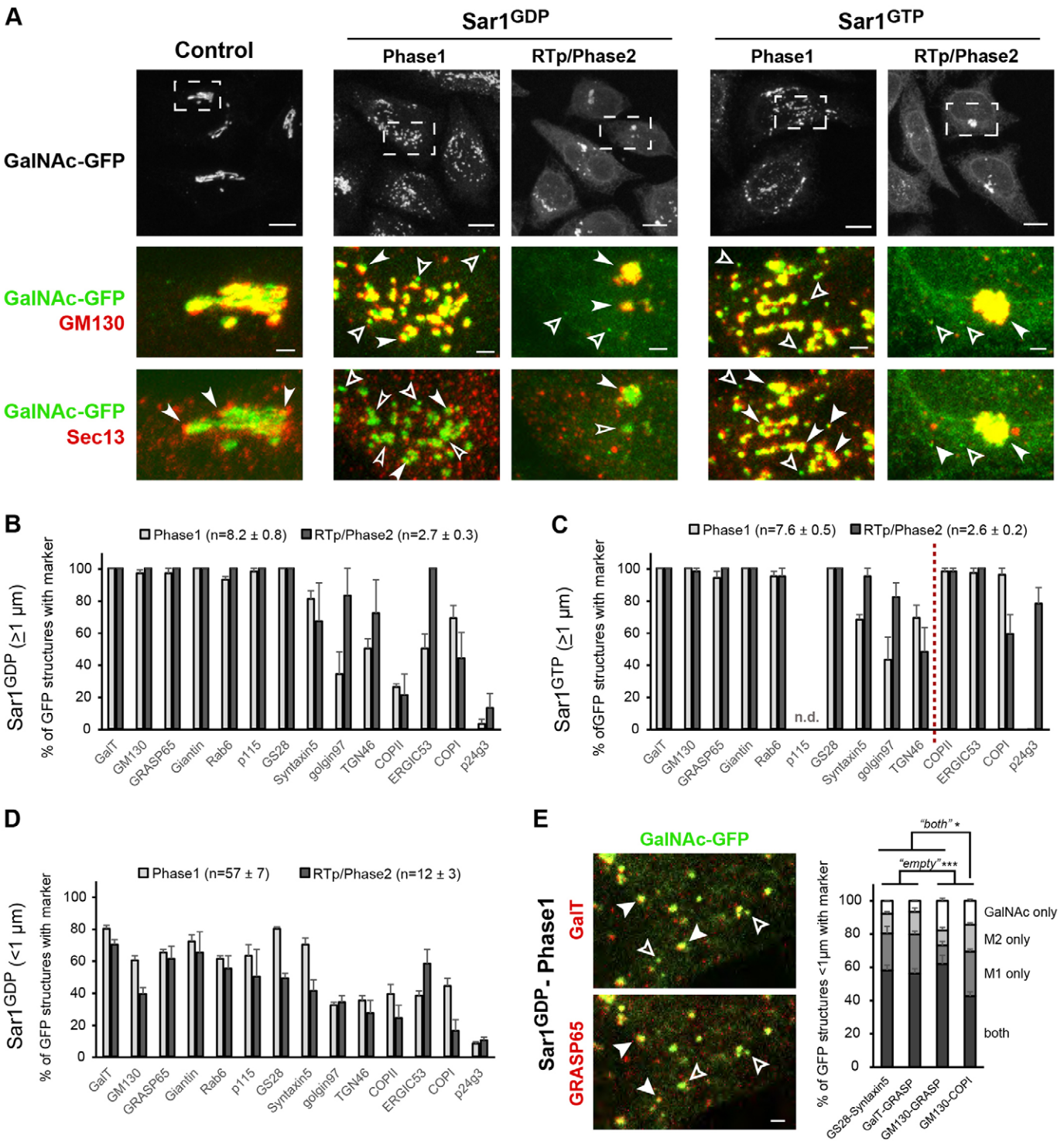

Fig. 5. GalNAc-T2–GFP fragments generated by Sar1 mutant expression display Golgi identity. HeLa cells stably expressing GalNAc-T2–GFP were infected with $Sar1^{GTP}$ (A,C) or $Sar1^{GDP}$ (A,B,D,E) adenoviruses, fixed at the indicated time-points and immunostained with the indicated antibodies. (A) Untreated cells, cells representative of phase1 and of Golgi remnant time-point (RTp)/phase2 were selected to compare the overlap of Sec13 and GM130 signal on GalNAc-T2–GFP structures. (A,E) Closed and open arrowheads indicate GalNAc-T2–GFP structures with or without signal overlap of the indicated marker, respectively. Long and short arrowheads indicate large and small GalNAc-T2-GFP structures, respectively. (B–E) Quantification of signal overlap of the indicated antibody staining with GFP signal on large (≥1 µm diameter) or small (<1 µm) GalNAc-T2–GFP structures. Values plotted are the mean±s.e.m. (B–D) Four different cells were analyzed, *n* indicates the average number (mean±s.e.m.) of GalNAc-T2–GFP structures per cell for different breakdown phases. n.d., not determined. (E) Four cells in phase 1 were analyzed. GS28/Syntaxin5, $n=259$; GalT/GRASP65, $n=257$; GM130/GRASP65, $n=196$; GM130/COPI, $n=366$. M1, marker 1 (GS28, GalT or GM130); M2, marker 2 (Syntaxin5, GRASP65 or COPI). $^{*}P<0.05$; $^{***}P<0.01$ (two-tailed Student's *t*-test). Scale bars: 10 µm (A,E), 2 µm (A, zoom).

Journal of Cell Science (2015) 128, 1279–1293 doi:10.1242/jcs.154443

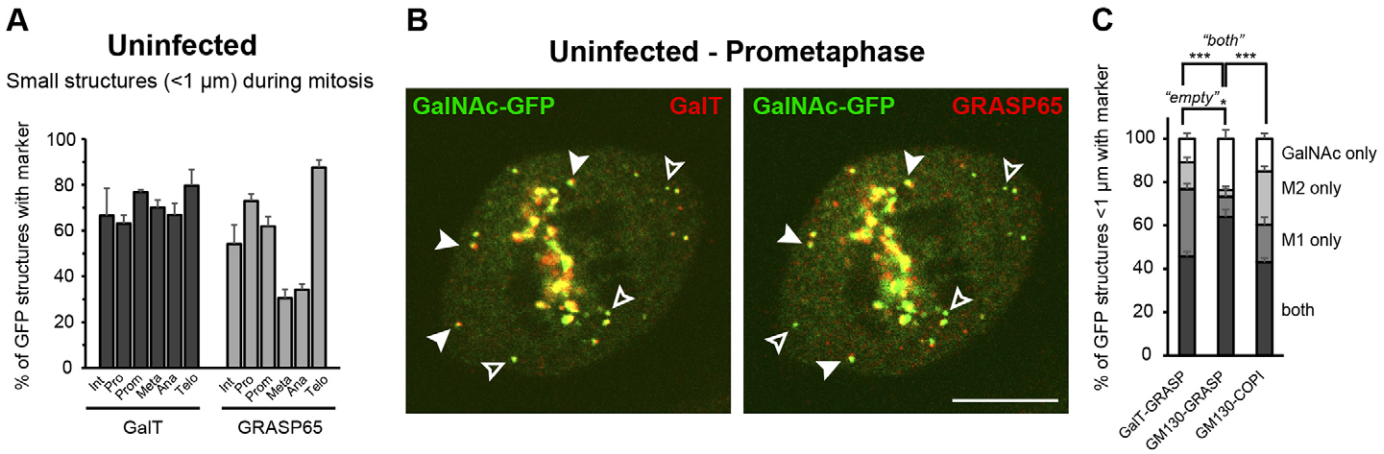

Fig. 6. Molecular composition of small GalNAc-T2–GFP fragments during cell division. HeLa cells stably expressing GalNAc-T2–GFP were fixed and immunostained with the indicated antibodies. (A) Three to six cells for each mitotic stage were analyzed for GalT and GRASP65 marker overlap with the GalNAc-T2–GFP signal (interphase, $n=11$, $n=18$; prophase, $n=64$, $n=131$; prometaphase, $n=130$, $n=227$; metaphase, $n=71$, $n=173$; anaphase, $n=144$, $n=288$; telophase (cells combined), $n=97$, $n=190$ for GalT and GRASP65, respectively). (B,C) Cells in prometaphase were analyzed for co-staining with the indicated antibodies. (B) Closed and open arrowheads indicate GalNAc-T2–GFP structures with or without signal overlap for GalT and GRASP65, respectively. Scale bar: 10 µm. (C) Four cells in prometaphase were analyzed for co-labeling of GalT/GRASP65, $n=130$; GM130/GRSP65, $n=97$; GM130/COPI, $n=137$. M1, marker 1 (GalT or GM130); M2, marker 2 (GRASP65 or COPI). Data show the mean±s.e.m.; $^{*}P<0.05$; $^{***}P<0.01$ (two-tailed Student's *t*-test).

found (Fig. 6C). This indicates that distinct subclasses of small Golgi fragments are generated during mitosis, a result similar to what we have obtained for Sar1-mutant-induced Golgi breakdown. We then decided to assess the physiological properties of Golgi breakdown intermediates generated after ER export block by analyzing their behavior during cell division. It has been shown that cells are able to divide during BFA treatment or upon Sar1 mutant microinjection (Nizak et al., 2004; Prescott et al., 2001; Seemann et al., 2002; Zaal et al., 1999). When we analyzed $Sar1^{GTP}$-virus-infected cells we could confirm that cells still divided at different time-points after virus infection. Notably, the time needed for completing mitosis after prometaphase was the same for uninfected and virus-infected cells – 72±24 min ($n=47$) and 72±33 min ($n=111$; ±s.d.), respectively. When we scored for mitotic indices, we obtained slightly higher values for $Sar1^{GTP}$-infected cells (0.044±0.024 at 4 h and 0.029±0.018 at 7 h post-infection; mean±s.d., $n=3$) and slightly smaller values for $Sar1^{GDP}$-infected cells (0.011±0.004 at 5 h and 0.012±0.003 at 8 h post-infection; $n=3$) compared to uninfected cells (0.019±0.013; $n=5$). Although interesting in terms of how transport activities might influence cell division, we did not study these differences in more detail. Next, we imaged virus-infected cells over time with a *z*-depth of ~35 µm and identified mitotic events during Golgi breakdown. For control cells, we observed Golgi fragmentation, redistribution and subsequent reassembly of Golgi twins at the spindle poles and former midbody region (supplementary material Fig. S4A) as has been described previously (Gaietta et al., 2006; Jesch and Linstedt, 1998; Shima et al., 1997). Remarkably, we observed a very similar behavior of the Golgi breakdown intermediates in cells expressing Sar1 mutants (Fig. 7). For example, in $Sar1^{GTP}$-expressing cells in breakdown phase 1, we observed that the already fragmented Golgi broke apart into even smaller structures that reorganized in each daughter cell on two sites after cell division (Fig. 7A). However, the reformed Golgi structures disintegrated over time until all GalNAc-T2–GFP material was redistributed to the ER (Fig. 7A). When following a $Sar1^{GDP}$-expressing cell entering mitosis (with Golgi remnant), we also observed smaller GFP structures during metaphase and re-clustering of Golgi material in the daughter cells after cell division (Fig. 7B). Again, the reformed structures continued to dissolve until all GalNAc-T2–GFP was redistributed to the ER (Fig. 7B). The continued Golgi redistribution after mitosis indicated that the ER export block remained stable during cell division. To confirm this, we analyzed VSVG–YFP fluorescence signal in $Sar1^{GTP}$-expressing cells and indeed did not find any distinct post-ER VSVG–YFP structures appearing during or after cell division (supplementary material Fig. S1F). To quantify the dynamics of GalNAc-T2–GFP fragments during mitosis, we analyzed the obtained movies with MorphoQuant (supplementary material Fig. S4). The area of the largest fragments was again used to generate a measure for Golgi breakdown when entering mitosis (B/A) and to score for re-clustering after mitosis (C/B) (Fig. 7; supplementary material Fig. S4). Uninfected cells displayed very pronounced breakdown and re-clustering indices of 0.02±0.01 and 107±20, respectively (Fig. 7C,D). Importantly, similar values were found for virus-infected cells that went into mitosis before the start of Golgi breakdown (Fig. 7C,D 'before'), i.e. virus infection per se does not influence Golgi dynamics. For cells entering mitosis during Golgi breakdown, the majority of cells scored breakdown indices smaller than 1.0 and re-clustering values larger than 1.0 (Fig. 7C,D). When we compared the mean values for the area sizes of Golgi fragments in mitosis, we found that they were usually bigger for $Sar1^{GTP}$-expressing cells compared with those of untreated cells (Fig. 7E). By contrast, for $Sar1^{GDP}$-expressing cells this effect could only be observed in phase 2 cells (Fig. 7B, metaphase; Fig. 7C), indicating minor differences between the mutants in how well Golgi fragment disintegration worked during mitosis. Taken together, the analysis reveals that Golgi breakdown intermediates generated by ER export block are still able to be dis- and reassembled in a regulated manner following cell division.

In summary, our study shows that Golgi breakdown in $Sar1^{GTP}$- and $Sar1^{GDP}$-expressing cells occurs in two phases

Journal of Cell Science (2015) 128, 1279–1293 doi:10.1242/jcs.154443

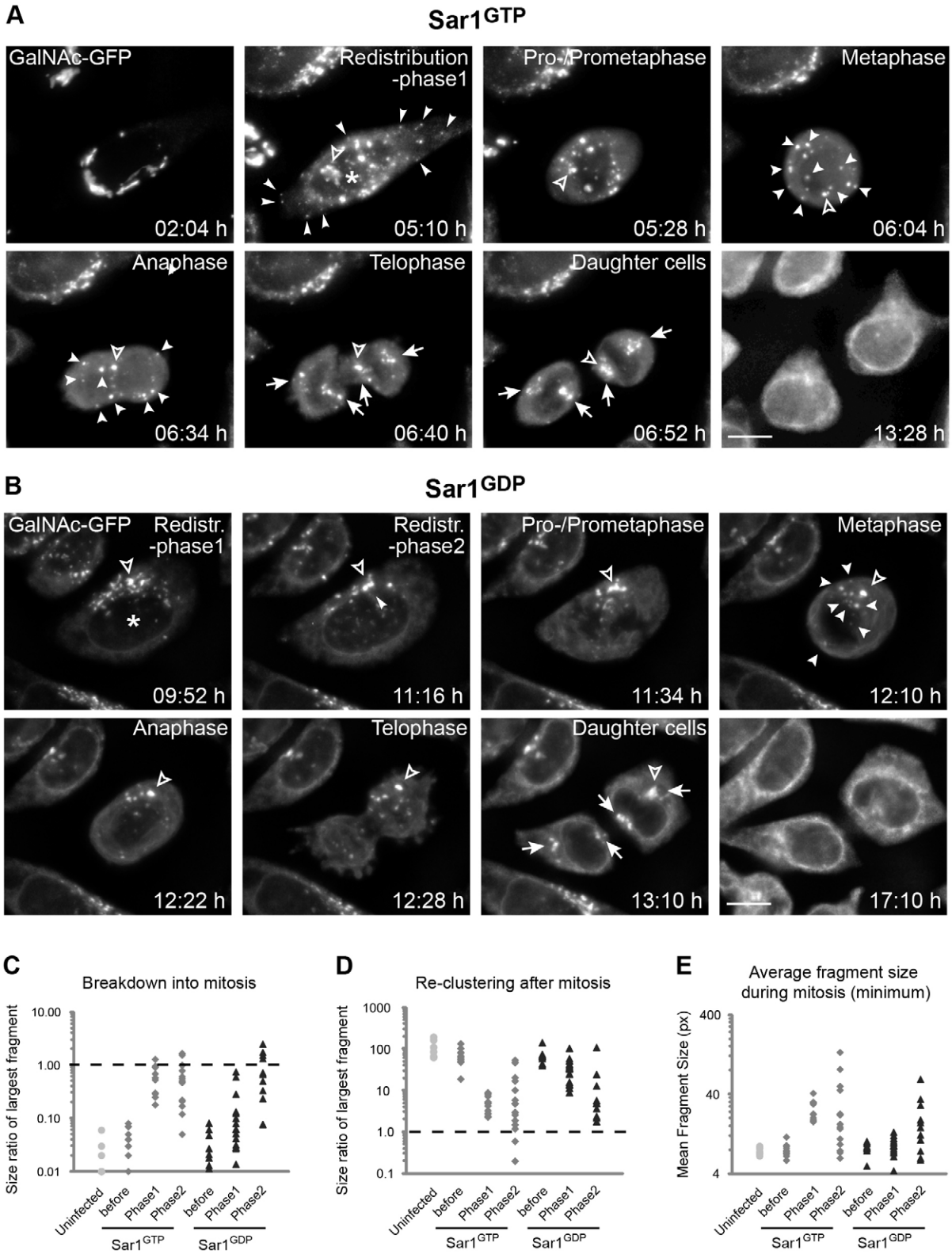

Fig. 7. See next page for legend.

with prominent self-organization activities of Golgi breakdown intermediates. The breakdown intermediates lack important components for cisternal shaping, they lost BFA sensitivity, ER recycling cargo and most probably their secretory cargo; yet they still display Golgi identity. We therefore conclude that the Golgi breakdown intermediates represent 'core' Golgi material that provides a previously unknown layer of Golgi self-organization that works independently of transport from the ER.

Journal of Cell Science (2015) 128, 1279–1293 doi:10.1242/jcs.154443

Fig. 7. Dynamics of Golgi fragments during cell division after Sar1 mutant expression. HeLa cells stably expressing GalNAc-T2–GFP were infected with $Sar1^{GTP}$ (A) or $Sar1^{GDP}$ viruses (B) and imaged on a fluorescence microscope for 12 h in a *z*-range of ~35 µm; time-points are post virus infection. (A,B) Asterisks indicate GalNAc-T2–GFP redistribution that has started; long arrowheads in A indicate peripheral GalNAc-T2–GFP fragments characteristic of phase 1. The long arrowhead in B indicates the site of Golgi remnant reformation. Short arrowheads point to unresolved GalNAc-T2–GFP fragments during mitosis; open arrowheads indicate the largest GalNAc-T2–GFP fragment identified; arrows indicate sites of Golgi reformation after mitosis. Scale bars: 10 µm. (C,D) The fragmentation ratio into mitosis and the re-clustering ratio after mitosis were determined for uninfected cells ($n=7$) and $Sar1^{GTP}$- or $Sar1^{GDP}$-virus-infected cells before Golgi fragmentation ($n=10$ and $n=9$), cells in phase 1 ($n=10$ and $n=17$) and cells at RTp/in phase 2 ($n=15$ and $n=11$) of Golgi breakdown. (E) The minimum of the mean area of Golgi fragments during mitosis was scored as the number of pixels (px). (C–E) Circles represent uninfected cells, diamonds and triangles represent cells expressing $Sar1^{GTP}$ and $Sar1^{GDP}$, respectively.

DISCUSSION

Studies on Golgi breakdown after ER export block have so far mainly highlighted the differences in $Sar1^{GTP}$ versus $Sar1^{GDP}$ expression on Golgi organization, leading to a lack of clarity on the extent to which Golgi organization depends on ER-to-Golgi transport (Miles et al., 2001; Prescott et al., 2001; Seemann et al., 2000; Seemann et al., 2002; Shima et al., 1998; Storrie et al., 1998; Stroud et al., 2003; Ward et al., 2001; Yoshimura et al., 2004; Zaal et al., 1999). However, one would not expect that different modes of blocking the same process, i.e. COPII-dependent ER export, should affect the Golgi, an organelle distinct from the ER, so differently. Using a systematic live-cell imaging analysis of Golgi breakdown over time, we find that the pattern of Golgi breakdown for the two Sar1 mutants is remarkably very similar. The major difference lies in the accumulation of COPII coat on Golgi fragments as a consequence of $Sar1^{GTP}$-mediated inhibition of uncoating COPII vesicles. Apparently, this causes other Golgi and transport markers to concentrate on the fragments, and results in the clustering of certain Golgi markers. By contrast, $Sar1^{GDP}$ blocks the formation of new COPII vesicles and therefore leads to a dispersed appearance of COPII coat components. As a consequence, we observe at the final time-point of our assay the pronounced differences between $Sar1^{GTP}$ and $Sar1^{GDP}$ that have been reported previously (supplementary material Fig. S3) (Seemann et al., 2000; Seemann et al., 2002; Stroud et al., 2003; Ward et al., 2001; Yoshimura et al., 2004; Zaal et al., 1999). Further (minor) differences between the Sar1 mutants can be found in Golgi breakdown kinetics (Table 1). Some, like the higher re-clustering efficiency for $Sar1^{GTP}$-expressing cells and the prolonged phase 2, could be explained by tight COPII coat association with Golgi fragments. Others might arise because the $Sar1^{GTP}$ mutant is faster and more efficient at establishing a robust ER export block; for example, the earlier starting point and the more synchronous phase 1. Importantly, we find for both Sar1 mutants a similar Golgi breakdown pattern – a biphasic process in which the breakdown intermediates show substantial self-organization abilities. The self-organization activities are reinforced by several findings – a microtubule-dependent re-clustering of Golgi fragments in the perinuclear area, the fusion of the membrane-bound structures that they contain and the ability to disassemble during and reassemble after cell division. Obviously, components important for these processes are still present on Golgi breakdown intermediates and, indeed, we find a large range of typical Golgi markers on the reformed Golgi remnant. Thus, we have identified 'core' Golgi material that provides a layer of Golgi self-organization independent of ER-to-Golgi transport.

The core Golgi material seems to be recognized and actively transported by the microtubule network. How is the association of Golgi structures with microtubules organized on the molecular level? One possibility could involve previously described Golgi-microtubule linker proteins such as GMAP210 (also known as TRIP11) and AKAP450 (also known as CG-NAP or AKAP9), but also Golgi-membrane-dependent microtubule nucleation activities might play a role (Infante et al., 1999; Kim et al., 2007; Ríos et al., 2004; Rivero et al., 2009). Remarkably, we found first an extensive fragmentation of the Golgi in phase 1 and the microtubule-dependent re-clustering of the Golgi material only later, suggesting that normal Golgi–microtubule interactions are initially lost after stopping ER export and are re-established later. Possible causes for this might be found in the loss of fast recycling material and/or the loss of cisternal morphology that occur in parallel.

In contrast to the cisternal shape morphology, the stacking function of the core Golgi material seems to be retained. By using electron microscopy, we found that the vesicle-like structures tightly associated with each other, forming distinct clusters in the cell. In addition, typical Golgi stacking factors like GRASP65 were present on Golgi breakdown intermediates. As clusters of vesicular structures have been described as units of Golgi inheritance (Jokitalo et al., 2001; Lucocq et al., 1987; Misteli and Warren, 1995; Shima et al., 1997), it seems possible that the vesicular clusters that we observed during Sar1-mutant-induced Golgi breakdown represent similar units of Golgi organization. We found even further similarities when analyzing the molecular composition of these clusters; during both events distinct subclasses of Golgi-derived fragments are generated. However, to what extent these fragments are comparable will require a more detailed analysis. The rapid formation of vesicular clusters after ER export block could nevertheless reflect an early step of the mitotic inheritance pathway of the Golgi, as ER-to-Golgi transport is shut off during cell division (Farmaki et al., 1999; Prescott et al., 2001). Similar to Sar1-mutant-induced breakdown, Golgi fragmentation before mitosis occurs rapidly, within ~30 min (Fig. 6; supplementary material Fig. S3) (Gaietta et al., 2006). Before cell division, the additional involvement of mitosis-specific steps, e.g. the phosphorylation of certain Golgi proteins, might further assist the disintegration of larger Golgi fragments (Acharya et al., 1998; Duran et al., 2008; Lin et al., 2000; Preisinger et al., 2005; Sütterlin et al., 2001; Yoshimura et al., 2005). In Sar1-mutant-expressing cells, further disintegration of initially generated Golgi fragments takes substantially more time. However, we observed mitotic disassembly of these fragments when Sar1-mutant-expressing cells were dividing, and even when the fragments had been generated hours before mitosis. This suggests that regulatory components important for (re)organization of the Golgi during mitosis are permanently present on Golgi breakdown intermediates. Interestingly, a previous study showed that BFA-resistant Golgi remnants are (re)assembled in daughter cells when the drug is added to metaphase cells (Nizak et al., 2004). As we found Golgi breakdown intermediates to be BFA resistant (and able to reassemble after mitosis), it is possible that both represent the same type of core Golgi material that promotes Golgi self-organization. To further investigate this core Golgi might therefore be very interesting.

MATERIALS AND METHODS

Cell culture and adenovirus infection

HeLa cells and HeLa cells stably expressing GalNAc-T2–GFP (Storrie et al., 1998) were grown in Dulbecco's modified Eagle medium (DMEM, Gibco) supplemented with 10% fetal bovine serum (FBS, PAA), 1% L-glutamine and 0.5 mg/ml geneticin (Gibco) at 37℃ under 5% CO_2. Usually, 30,000 cells/ml were seeded on glass-bottomed dishes (MatTek) or four-well LabTek dishes (Nunc) and incubated for 24 h or 48 h before virus infection. Adenovirus infections were performed for 1 h at 37℃ in 500 µl of DMEM or 100 µl of DMEM for MatTek or four-well LabTek dishes, respectively. Double infections with the Cre recombinase and Sar1(H79G) or Sar1(T39N) adenoviruses [kind gift of Nobuhiro Nakamura, Kyoto Sangyo University (Yoshimura et al., 2004)] were performed with a multiplicity of infection (MOI) of ~5000 for each virus, control infections using single adenoviruses were performed with MOIs of ~10,000.

Antibodies

The primary antibodies used for immunofluorescence were as follows: mouse anti-FLAG (M2, Sigma), mouse anti-KDEL receptor (Calbiochem), mouse anti-GM130, mouse anti-Sec31 and mouse anti-GS28 (BD Biosciences), rabbit anti-Rab6 (Santa Cruz Biotechnology), rabbit anti-giantin (Abcam), mouse anti-GalT (Cellmab), mouse anti-golgin97 (Molecular Probes), rabbit anti-GRASP65 (Abcam), rabbit anti-syntaxin5 (Synaptic Syst.), sheep anti-TGN46 (Serotec), sheep anti-GRASP65 (kind gift of Martin Lowe, University of Manchester, UK) and mouse anti-ERGIC53 (kind gift of Hans-Peter Hauri, University of Basel, Switzerland). Rabbit antibodies against recombinant p24γ3(p27), β′-COPI and Sec13 were raised by standard protocols and have been described previously (Simpson et al., 2006; Simpson et al., 2012). The secondary antibodies used for immunofluorescence were as follows: Alexa-Fluor-568-conjugated goat anti-mouse-IgG and goat anti-rabbit-IgG, Alexa-Fluor-647-conjugated donkey anti-sheep-IgG (Molecular Probes) and Cy5-conjugated goat anti-rabbit-IgG (GE Healthcare). The antibodies used for western blot analysis were as follows: mouse anti-FLAG (M2, Sigma), anti-α-tubulin (Neomarkers) and HRP-conjugated goat anti-mouse-IgG antibody (Sigma).

VSVG–YFP transport assay

HeLa cells were infected with a VSVG–YFP-encoding adenovirus (Keller et al., 2001) for 1 h at 37℃ and incubated for 2–3 h at 37℃. Cells were then infected for 1 h at 37℃ with Sar1 mutant virus alone or in combination with Cre viruses with MOIs as above and subsequently shifted to 39.5℃ for 3.5 h. To release the temperature-dependent transport block, cells were incubated and directly imaged alive at 32℃ on a Leica widefield fluorescence microscope system (see below) to follow VSVG–YFP transport and localization.

Fluorescence microscopy and image analysis

Time-lapse imaging was performed on Leica AF6000/AF7000 widefield microscopy systems with 63× glycerol (HCX PL APO, NA 1.30) or 40× air (PL FLUOTAR L, NA 0.60) objectives using filter settings for GFP or YFP illumination and detection. Cells were kept at 37℃ and 5% CO_2 in imaging medium containing Na_2CO_3 (prepared in-house). Images were acquired with a 12-bit camera (DFC350 FX R2) on single *z*-planes (Fig. 1A; Fig. 4D; supplementary material Figs S1, S2) or as *z*-stacks that were maximum intensity projected: three slices with $\Delta z=2$ µm for Fig. 2A,E, and 53–55 slices with $\Delta z=0.59$ µm after deconvolution by Huygens software for Fig. 7A,B and supplementary material Fig. S4A. Images in Fig. 1B were acquired on a PerkinElmer UltraVIEW RS system with 100× oil objective (Zeiss PLAN-APOCHROMAT, NA 1.4) and 488-nm laser illumination. Five slices with $\Delta z=0.30$ µm were maximum intensity projected. The gamma value of GFP signal was enhanced in time-lapse imaging galleries to better visualize ER fluorescence. For signal analysis of GalNAc-T2–GFP movies with MorphoQuant, regions of single cells were selected and all raw images of the time series were segmented individually to identify and measure Golgi structures (see below).

Image analysis with MorphoQuant

We developed a Matlab-based image-processing algorithm, MorphoQuant, which detects both locally bright large objects of arbitrary shape and locally bright small dot-like objects (supplementary material; https://github.com/tischi/MorphoQuant). First, the algorithm separates the Golgi foreground from the ER background by a morphological top-hat filter whose size parameter was adapted to the size of the largest Golgi objects. The resulting foreground image was subjected to a local adaptive threshold algorithm yielding a reliable segmentation of larger Golgi structures. To enhance detection of small dot-like structures in the same image, we convolved the foreground image with a Laplacian of Gaussian kernel whose size parameter was set to match vesicle sizes. Local adaptive thresholding of the convolved foreground image yielded reliable detection of small dot-like structures. Finally, we combined the results of both segmentation steps and assigned objects with more than six pixels as valid Golgi structures, whereas smaller objects were rejected as noise. The accuracy of the segmentation was assessed by visual inspection and the thresholds were adjusted to minimize the detection of false-positive structures.

Co-immunofluorescence analysis

HeLa cells stably expressing GalNAc-T2–GFP were infected with $Sar1^{dn}$ and Cre viruses and fixed at the indicated time-points with methanol at −20℃ for 4 min or with 3% paraformaldehyde at room temperature for 20 min. PFA-fixed cells were incubated in PBS+0.1% Triton X-100 or 0.05% saponin+BSA for 10 min. Cells were incubated for 1 h with primary antibodies, washed for 10 min, and incubated for 45 min with secondary antibodies and for 10 min with Hoechst 33342 to stain nuclei. Images were taken on a Zeiss LSM710/780 laser-scanning confocal microscope with a 63× oil objective (Plan Apochromat, NA 1.40, DIC M27) with different zoom factors, and cells were imaged in the range of ~0.11-µm resolution in the *xy*-axis and 0.34 µm in the *z*-axis. The pinhole was opened to ~1 airy unit. Images were scanned in sequential mode with laser lines of 405 nm, 488 nm, 561 nm and 633 nm, and the corresponding detection settings. Images shown in Fig. 4C and Fig. 5A,G are single *z*-planes, in Fig. 4A maximum intensity and in Fig. 4B sum projections of *z*-stacks. Quantification of colocalization was performed by visual inspection of single planes for at least four cells with representative Golgi morphologies and scored positive when >10% of the area was covered by the marker. Small and large (<1 µm or ≥1 µm, respectively) structures were distinguished by measuring the largest diameter of the structure.

Correlative fluorescence and electron microscopy

HeLa cells stably expressing GalNAc-T2–GFP were seeded in MatTek dishes 24–48 h prior to the experiment. Cells were co-infected with single $Sar1^{dn}$ or $Sar1^{dn}$ and Cre viruses and transferred to a widefield microscope (Olympus CellR) at the indicated time-points after infection in CO_2-independent imaging medium (Gibco). Representative cells for each time-point were marked by inscriptions within the glass coverslip using a 355-nm pulsed laser (Colombelli et al., 2008). Transmission and fluorescent images were acquired and the cells fixed immediately in 2.5% glutaraldehyde. The samples were flat embedded in Epon and processed for electron microscopy as described previously (Colombelli et al., 2008). Whole cell volumes were analyzed for Golgi remnants or vesicular clusters by visual inspection of ultrathin serial sections (50–60 nm) using a transmission electron microscope (CM120 Biotwin, FEI). Two to three cells for each time-point were chosen and fluorescent GalNAc-T2–GFP structures from maximum projections of the live-cell images were correlated with vesicular clusters on the micrograph pictures. First, the total number of clusters per cell was assessed (defined as >30 closely associated vesicular structures). Then, the number and diameter of vesicles in each cluster was measured.

Acknowledgements

We thank Olympus Europe, Carl Zeiss, Leica Systems and the ALMF team at EMBL Heidelberg for continuous support. In addition, we thank Uta Hasemann-Weiss and the EM core facility at EMBL Heidelberg for their help with electron microscopy. We are grateful to Nobuhiro Nakamura (Kyoto Sangyo University) for providing Cre and Sar1 mutant viruses. We thank Roland Wedlich-Söldner, Joe Lewis and members of the Pepperkok lab for comments on the manuscript.

Competing interests
The authors declare no competing or financial interests.

Author contributions
C.E.S. and R.P. conceived of the study, designed the experiments and wrote the manuscript. C.E.S., C. Taengemo and C.C. performed experiments and analyzed the data. C. Tischer analyzed data and developed the MorphoQuant software.

Funding
C.E.S. was supported by an EMBO long-term fellowship [grant number ALTF 168-2007].

Supplementary material
Supplementary material available online at
http://jcs.biologists.org/lookup/suppl/doi:10.1242/jcs.154443/-/DC1

References
Acharya, U., Mallabiabarrena, A., Acharya, J. K. and Malhotra, V. (1998). Signaling via mitogen-activated protein kinase kinase (MEK1) is required for Golgi fragmentation during mitosis. *Cell* **92**, 183-192.
Blum, R., Pfeiffer, F., Feick, P., Nastainczyk, W., Kohler, B., Schäfer, K. H. and Schulz, I. (1999). Intracellular localization and in vivo trafficking of p24A and p23. *J. Cell Sci.* **112**, 537-548.
Colombelli, J., Tängemo, C., Haselman, U., Antony, C., Stelzer, E. H., Pepperkok, R. and Reynaud, E. G. (2008). A correlative light and electron microscopy method based on laser micropatterning and etching. *Methods Mol. Biol.* **457**, 203-213.
Derby, M. C. and Gleeson, P. A. (2007). New insights into membrane trafficking and protein sorting. *Int. Rev. Cytol.* **261**, 47-116.
Donaldson, J. G., Lippincott-Schwartz, J., Bloom, G. S., Kreis, T. E. and Klausner, R. D. (1990). Dissociation of a 110-kD peripheral membrane protein from the Golgi apparatus is an early event in brefeldin A action. *J. Cell Biol.* **111**, 2295-2306.
Duran, J. M., Kinseth, M., Bossard, C., Rose, D. W., Polishchuk, R., Wu, C. C., Yates, J., Zimmerman, T. and Malhotra, V. (2008). The role of GRASP55 in Golgi fragmentation and entry of cells into mitosis. *Mol. Biol. Cell* **19**, 2579-2587.
Farmaki, T., Ponnambalam, S., Prescott, A. R., Clausen, H., Tang, B. L., Hong, W. and Lucocq, J. M. (1999). Forward and retrograde trafficking in mitotic animal cells. ER-Golgi transport arrest restricts protein export from the ER into COPII-coated structures. *J. Cell Sci.* **112**, 589-600.
Füllekrug, J., Suganuma, T., Tang, B. L., Hong, W., Storrie, B. and Nilsson, T. (1999). Localization and recycling of gp27 (hp24γ3): complex formation with other p24 family members. *Mol. Biol. Cell* **10**, 1939-1955.
Gaietta, G. M., Giepmans, B. N., Deerinck, T. J., Smith, W. B., Ngan, L., Llopis, J., Adams, S. R., Tsien, R. Y. and Ellisman, M. H. (2006). Golgi twins in late mitosis revealed by genetically encoded tags for live cell imaging and correlated electron microscopy. *Proc. Natl. Acad. Sci. USA* **103**, 17777-17782.
Girod, A., Storrie, B., Simpson, J. C., Johannes, L., Goud, B., Roberts, L. M., Lord, J. M., Nilsson, T. and Pepperkok, R. (1999). Evidence for a COP-I-independent transport route from the Golgi complex to the endoplasmic reticulum. *Nat. Cell Biol.* **1**, 423-430.
Infante, C., Ramos-Morales, F., Fedriani, C., Bornens, M. and Rios, R. M. (1999). GMAP-210, A cis-Golgi network-associated protein, is a minus end microtubule-binding protein. *J. Cell Biol.* **145**, 83-98.
Jesch, S. A. and Linstedt, A. D. (1998). The Golgi and endoplasmic reticulum remain independent during mitosis in HeLa cells. *Mol. Biol. Cell* **9**, 623-635.
Jokitalo, E., Cabrera-Poch, N., Warren, G. and Shima, D. T. (2001). Golgi clusters and vesicles mediate mitotic inheritance independently of the endoplasmic reticulum. *J. Cell Biol.* **154**, 317-330.
Kasap, M., Thomas, S., Danaher, E., Holton, V., Jiang, S. and Storrie, B. (2004). Dynamic nucleation of Golgi apparatus assembly from the endoplasmic reticulum in interphase hela cells. *Traffic* **5**, 595-605.
Keller, P., Toomre, D., Díaz, E., White, J. and Simons, K. (2001). Multicolour imaging of post-Golgi sorting and trafficking in live cells. *Nat. Cell Biol.* **3**, 140-149.
Kim, H. S., Takahashi, M., Matsuo, K. and Ono, Y. (2007). Recruitment of CG-NAP to the Golgi apparatus through interaction with dynein-dynactin complex. *Genes Cells* **12**, 421-434.
Klumperman, J. (2011). Architecture of the mammalian Golgi. *Cold Spring Harb. Perspect. Biol.* **3**.
Lin, C. Y., Madsen, M. L., Yarm, F. R., Jang, Y. J., Liu, X. and Erikson, R. L. (2000). Peripheral Golgi protein GRASP65 is a target of mitotic polo-like kinase (Plk) and Cdc2. *Proc. Natl. Acad. Sci. USA* **97**, 12589-12594.
Lippincott-Schwartz, J., Yuan, L. C., Bonifacino, J. S. and Klausner, R. D. (1989). Rapid redistribution of Golgi proteins into the ER in cells treated with brefeldin A: evidence for membrane cycling from Golgi to ER. *Cell* **56**, 801-813.
Lowe, M. (2011). Structural organization of the Golgi apparatus. *Curr. Opin. Cell Biol.* **23**, 85-93.
Lucocq, J. M., Pryde, J. G., Berger, E. G. and Warren, G. (1987). A mitotic form of the Golgi apparatus in HeLa cells. *J. Cell Biol.* **104**, 865-874.
Miles, S., McManus, H., Forsten, K. E. and Storrie, B. (2001). Evidence that the entire Golgi apparatus cycles in interphase HeLa cells: sensitivity of Golgi matrix proteins to an ER exit block. *J. Cell Biol.* **155**, 543-556.
Misteli, T. and Warren, G. (1995). Mitotic disassembly of the Golgi apparatus in vivo. *J. Cell Sci.* **108**, 2715-2727.
Nakamura, N., Wei, J. H. and Seemann, J. (2012). Modular organization of the mammalian Golgi apparatus. *Curr. Opin. Cell Biol.* **24**, 467-474.
Nizak, C., Sougrat, R., Jollivet, F., Rambourg, A., Goud, B. and Perez, F. (2004). Golgi inheritance under a block of anterograde and retrograde traffic. *Traffic* **5**, 284-299.
Orci, L., Tagaya, M., Amherdt, M., Perrelet, A., Donaldson, J. G., Lippincott-Schwartz, J., Klausner, R. D. and Rothman, J. E. (1991). Brefeldin A, a drug that blocks secretion, prevents the assembly of non-clathrin-coated buds on Golgi cisternae. *Cell* **64**, 1183-1195.
Pavelka, M., Neumüller, J. and Ellinger, A. (2008). Retrograde traffic in the biosynthetic-secretory route. *Histochem. Cell Biol.* **129**, 277-288.
Pecot, M. Y. and Malhotra, V. (2006). The Golgi apparatus maintains its organization independent of the endoplasmic reticulum. *Mol. Biol. Cell* **17**, 5372-5380.
Preisinger, C., Körner, R., Wind, M., Lehmann, W. D., Kopajtich, R. and Barr, F. A. (2005). Plk1 docking to GRASP65 phosphorylated by Cdk1 suggests a mechanism for Golgi checkpoint signalling. *EMBO J.* **24**, 753-765.
Prescott, A. R., Farmaki, T., Thomson, C., James, J., Paccaud, J. P., Tang, B. L., Hong, W., Quinn, M., Ponnambalam, S. and Lucocq, J. (2001). Evidence for prebudding arrest of ER export in animal cell mitosis and its role in generating Golgi partitioning intermediates. *Traffic* **2**, 321-335.
Presley, J. F., Cole, N. B., Schroer, T. A., Hirschberg, K., Zaal, K. J. and Lippincott-Schwartz, J. (1997). ER-to-Golgi transport visualized in living cells. *Nature* **389**, 81-85.
Puri, S., Telfer, H., Velliste, M., Murphy, R. F. and Linstedt, A. D. (2004). Dispersal of Golgi matrix proteins during mitotic Golgi disassembly. *J. Cell Sci.* **117**, 451-456.
Ríos, R. M., Sanchís, A., Tassin, A. M., Fedriani, C. and Bornens, M. (2004). GMAP-210 recruits gamma-tubulin complexes to cis-Golgi membranes and is required for Golgi ribbon formation. *Cell* **118**, 323-335.
Rivero, S., Cardenas, J., Bornens, M. and Rios, R. M. (2009). Microtubule nucleation at the cis-side of the Golgi apparatus requires AKAP450 and GM130. *EMBO J.* **28**, 1016-1028.
Sandoval, I. V., Bonifacino, J. S., Klausner, R. D., Henkart, M. and Wehland, J. (1984). Role of microtubules in the organization and localization of the Golgi apparatus. *J. Cell Biol.* **99** Suppl.:, S113-S118.
Scheel, J., Pepperkok, R., Lowe, M., Griffiths, G. and Kreis, T. E. (1997). Dissociation of coatomer from membranes is required for brefeldin A-induced transfer of Golgi enzymes to the endoplasmic reticulum. *J. Cell Biol.* **137**, 319-333.
Seemann, J., Jokitalo, E., Pypaert, M. and Warren, G. (2000). Matrix proteins can generate the higher order architecture of the Golgi apparatus. *Nature* **407**, 1022-1026.
Seemann, J., Pypaert, M., Taguchi, T., Malsam, J. and Warren, G. (2002). Partitioning of the matrix fraction of the Golgi apparatus during mitosis in animal cells. *Science* **295**, 848-851.
Shima, D. T., Haldar, K., Pepperkok, R., Watson, R. and Warren, G. (1997). Partitioning of the Golgi apparatus during mitosis in living HeLa cells. *J. Cell Biol.* **137**, 1211-1228.
Shima, D. T., Cabrera-Poch, N., Pepperkok, R. and Warren, G. (1998). An ordered inheritance strategy for the Golgi apparatus: visualization of mitotic disassembly reveals a role for the mitotic spindle. *J. Cell Biol.* **141**, 955-966.
Shorter, J. and Warren, G. (2002). Golgi architecture and inheritance. *Annu. Rev. Cell Dev. Biol.* **18**, 379-420.
Simpson, J. C., Nilsson, T. and Pepperkok, R. (2006). Biogenesis of Tubular ER-to-Golgi Transport Intermediates. *Mol. Biol. Cell* **17**, 723-737.
Simpson, J. C., Joggerst, B., Laketa, V., Verissimo, F., Cetin, C., Erfle, H., Bexiga, M. G., Singan, V. R., Hériché, J. K., Neumann, B. et al. (2012). Genome-wide RNAi screening identifies human proteins with a regulatory function in the early secretory pathway. *Nat. Cell Biol.* **14**, 764-774.
Storrie, B., White, J., Röttger, S., Stelzer, E. H., Suganuma, T. and Nilsson, T. (1998). Recycling of golgi-resident glycosyltransferases through the ER reveals a novel pathway and provides an explanation for nocodazole-induced Golgi scattering. *J. Cell Biol.* **143**, 1505-1521.
Stroud, W. J., Jiang, S., Jack, G. and Storrie, B. (2003). Persistence of Golgi matrix distribution exhibits the same dependence on Sar1p activity as a Golgi glycosyltransferase. *Traffic* **4**, 631-641.
Sütterlin, C., Lin, C. Y., Feng, Y., Ferris, D. K., Erikson, R. L. and Malhotra, V. (2001). Polo-like kinase is required for the fragmentation of pericentriolar Golgi stacks during mitosis. *Proc. Natl. Acad. Sci. USA* **98**, 9128-9132.
Tängemo, C., Ronchi, P., Colombelli, J., Haselmann, U., Simpson, J. C., Antony, C., Stelzer, E. H., Pepperkok, R. and Reynaud, E. G. (2011). A novel laser nanosurgery approach supports de novo Golgi biogenesis in mammalian cells. *J. Cell Sci.* **124**, 978-987.
Thyberg, J. and Moskalewski, S. (1985). Microtubules and the organization of the Golgi complex. *Exp. Cell Res.* **159**, 1-16.
Ward, T. H., Polishchuk, R. S., Caplan, S., Hirschberg, K. and Lippincott-Schwartz, J. (2001). Maintenance of Golgi structure and function depends on the integrity of ER export. *J. Cell Biol.* **155**, 557-570.

Journal of Cell Science

Wehland, J., Henkart, M., Klausner, R. and Sandoval, I. V. (1983). Role of microtubules in the distribution of the Golgi apparatus: effect of taxol and microinjected anti-alpha-tubulin antibodies. *Proc. Natl. Acad. Sci. USA* **80**, 4286-4290.

Wei, J. H. and Seemann, J. (2009). Mitotic division of the mammalian Golgi apparatus. *Semin. Cell Dev. Biol.* **20**, 810-816.

Wei, J. H. and Seemann, J. (2010). Unraveling the Golgi ribbon. *Traffic* **11**, 1391-1400.

Yoshimura, S., Yamamoto, A., Misumi, Y., Sohda, M., Barr, F. A., Fujii, G., Shakoori, A., Ohno, H., Mihara, K. and Nakamura, N. (2004). Dynamics of Golgi matrix proteins after the blockage of ER to Golgi transport. *J. Biochem.* **135**, 201-216.

Yoshimura, S., Yoshioka, K., Barr, F. A., Lowe, M., Nakayama, K., Ohkuma, S. and Nakamura, N. (2005). Convergence of cell cycle regulation and growth factor signals on GRASP65. *J. Biol. Chem.* **280**, 23048-23056.

Zaal, K. J., Smith, C. L., Polishchuk, R. S., Altan, N., Cole, N. B., Ellenberg, J., Hirschberg, K., Presley, J. F., Roberts, T. H., Siggia, E. et al. (1999). Golgi membranes are absorbed into and reemerge from the ER during mitosis. *Cell* **99**, 589-601.